Beam Collapse and Polarization Self-Modulation in an Optically Active Photorefractive Crystal in an Alternating Electric Field

C. A. Fuentes-Hernández and A. V. Khomenko

Optics Department, CICESE, Carretera Tijuana-Ensenada km. 107, A.P. 2732, Ensenada, B.C., México

(Received 10 November 1998)

Consistent experimental and numerical simulation studies of the propagation of a one-dimensional Gaussian beam in optically active BSO crystal in the presence of an alternating external field are presented. We have observed three forms of the beam evolution: (i) polarization-dependent self-bending, in which the crystal acts as a nonlinear polarization beam splitter; (ii) spatially nonuniform self-modulation of the state of polarization; (iii) formation of narrow inclined waveguides within the Gaussian beam. The effects of optical activity and the crystal orientation are discussed.

PACS numbers: 42.65.Hw, 42.65.Tg

In the past few years, nonlinear propagation of laser beams in photorefractive crystals has been extensively studied. In particular, steady-state spatial, bright, dark, and vortex solitons have attracted recent interest [1–4]. Stable propagation of spatial solitons requires a drift mechanism of photorefractive nonlinearity. On the other hand, a diffusion mechanism of nonlinearity provides other interesting possibilities for beam steering and confinement, namely, beam self-bending and propagation of nonlinear surface waves [5–8]. Many other important applications of photorefractive crystals involve the two-beam or multibeam interaction and require a photorefractive crystal with the diffusion-type mechanism of the space charge formation [9]. Our study is focused on the shape and polarization evolution of the beam in cubic, optically active photorefractive crystals such as sillenite crystals ($Bi_{12}SiO_{20}$ and $Bi_{12}TiO_{20}$). The most effective way to enhance the diffusion-type nonlinearity in sillenite crystals is the use of an external alternating electric field [10]. Previous discussions of beam propagation in sillenite crystals have tended to ignore the effects of the beam profile, optical activity, and/or birefringence induced by an alternating external field [5,11–15]. In this paper we present the results of experimental and numerical studies of Gaussian beam propagation in $Bi_{12}SiO_{20}$ (BSO) in the presence of an alternating external electric field. We show how the initially linearly polarized beam with Gaussian profile evolves within the crystal, suffering a transverse polarization modulation that is different for the positive and negative half-cycles of the applied field.

In many experiments performed with the photorefractive $BaTiO_3$ crystals, the beam evolution inside the crystal was traced by observing it through the upper facet of the sample [16]. We were unable to use this technique because of the low intensity of the beam and the high optical quality of the crystal used in our experiments. In this case the only available experimental data to analyze the beam evolution inside the crystal are the beam profiles exiting the crystal. Thus our study includes the numerical simulation of the beam propagation that demonstrates the beam evolution. Nevertheless, the experimental part of our study is essential because we have proven the validity of our numerical results in detailed comparison with the experimental data.

Our experiments were performed using a $1 \times 6 \times 8$ mm^3 BSO sample and the experimental arrangement shown in Fig. 1. The lateral faces of the sample (6×8 mm^2) were coated with gold-evaporated electrodes measuring 4×6 mm^2 with the long side parallel to the light propagation direction. A 43 Hz bipolar square-wave voltage was applied to the electrodes, creating an electric field along the crystalline [001] axis. A focused beam from a He-Ne laser ($\lambda = 632.8$ nm) propagated along the longest side, which is parallel to the [110] axis. The laser beam intensity was adjusted by a variable neutral filter (VF) to provide a crystal response time of approximately 2 sec, which is much larger than the alternating-field period (23 ms). The quarter-wave plate, $\lambda/4$, and polarizer (P) were used to control the polarization angle of the incoming light. The beam was focused with a spherical lens (SL) at the input plane of the crystal. At the same plane the beam was defocused in the vertical direction by a cylindrical lens (CL). Thus a one-dimensional Gaussian beam was directed onto a photorefractive crystal. Images of the beam at the output plane of the crystal and at the far field were recorded with a CCD camera through the polarization analyzer (A) or without it. The CCD camera was not synchronized with the high voltage supply. We recorded the time-averaged images using the multiple frame acquisition mode of the camera.

Figure 2a shows nine far-field distributions of the intensity recorded with CCD camera when the polarization

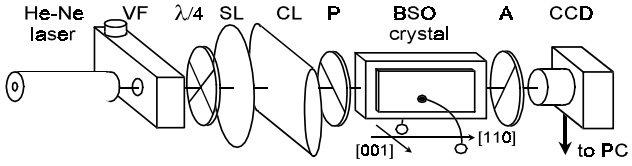

FIG. 1. Schematic of the experimental setup.

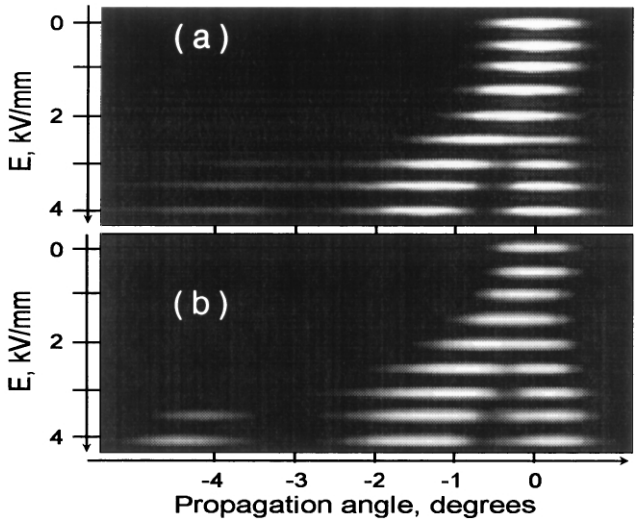

FIG. 2. Intensity of the light in the far field for different ac electric fields. (a) Experimental images; (b) results of numerical simulation.

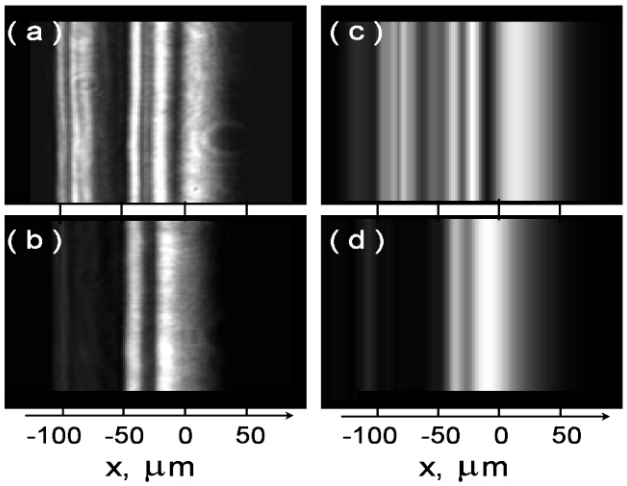

FIG. 3. Images of the beam in the output plane of the photorefractive crystal. Panels (a),(b) were recorded experimentally for the polarization orthogonal and parallel to the external electric field, respectively; (c) and (d) are the results of calculations by BPM.

analyzer, A, was removed from the experimental setup. The images were recorded for different amplitudes of the applied electric field with 0.5 kV/mm increments. The beam was focused near the input surface of the crystal to a waist of approximately 50 μm radius. We observed only one beam at the far field when the ac electric field amplitude was below 2 kV/mm. With such fields the beam self-bending could be detected, although it was almost negligible because the angular deviation of the beam did not surpass its angular divergence. With higher fields the beam is disintegrated and two or more beams appear in the far field. The beams in the far field had different polarization. For instance, when the amplitude of the ac electric field was 4 kV/mm, the beam located at $-1.5°$ was polarized almost linearly along the applied electric field (Fig. 2a). At the same time, the beam located in the image to the right of it had orthogonal polarization.

The images of the output crystal surface recorded with a CCD camera through a polarization analyzer are shown in Figs. 3a and 3b for light polarized parallel and perpendicular to the external field, respectively. The amplitude of the external electric field was 4 kV/mm. One can see that the image of the beam at the output crystal plane has bright, unequally spaced stripes. The width of the stripes is appreciably narrower than the beam-waist dimension in front of the crystal.

In this paper, for the first time to our knowledge, we apply the beam propagation method (BPM) to resolve a problem of beam polarization and shape evolution in a photorefractive crystal. We use the BPM modified for photorefractive crystals described in Ref. [8]. The parameters of the BSO crystal used in the calculations are low-frequency dielectric constant $\varepsilon = 56$, refractive index $n_o = 2.54$, electro-optic coefficient $r = 5$ pm/V, optical rotatory power $\rho = 21$ deg/mm, electron mobility lifetime product $\mu\tau = 10^{-7}$ cm^2/V, and effective trap concentration $N = 10^{16}$ cm^{-3} [17].

The results of our calculations are the two-dimensional distributions of the light amplitude. Two of them, $A_1(x, z)$ and $A_2(x, z)$, represent two orthogonal polarizations for the positive half-cycle of an ac electric field, whereas the other two, $A_3(x, z)$ and $A_4(x, z)$, are for the negative half-cycle. The coordinates x and z are in the transverse and longitudinal directions, respectively. Figure 2b shows the results of the calculation of the far-field intensity distributions for different amplitudes of the external ac field. In these calculations the beam had a 45° polarization and a 50-μm-dimension Gaussian profile in the input plane of the crystal. To compare these results with the experimental far-field images recorded without the polarization analyzer and with a CCD's exposure time that is much longer than the alternating-field period, each intensity distribution is calculated as the sum of intensities of both polarization components for the positive and negative electric field half-cycle,

$$I(\theta) = \frac{1}{2} \sum_{i=1}^{4} |F[A_i(x, L)]|^2, \qquad (1)$$

where F represents the fast Fourier transform and L is the length of the electrodes, $L = 6$ mm. For comparison with the experimental images, we present the calculated one-dimensional intensity distributions in Fig. 2b as images with the Gaussian profile in the vertical direction. Figure 3 shows the images of the beam in the output plane of the crystal for two orthogonal polarization components. The images were calculated as the sums of the intensities for the positive and negative electric field half-cycles. Figures 2 and 3 show an incontrovertible similarity between the experimental data and the results of the

calculations. We have found the same similarity for the results that were obtained for other polarization states and for different amplitudes of the applied ac electric field. The consistency of the experimental and numerical results proves the validity of the approximations that were made in calculations. In particular, any noise fanning effects have been neglected in our calculations and the validity of this assumption has been verified experimentally. We attribute this to the high optical quality of our BSO sample and to the small size of the beam, which allowed us to easily avoid occasional surface defects.

Now we show how the Gaussian beam evolves in the BSO crystal in the presence of an alternating external field. Figure 4 presents two-dimensional distributions of the light intensity in the xz plane. The ac external field of 4 kV/mm is applied along crystalline [001] axis; the beam has a waist of 50 μm and is focused at the input plane of the crystal. Note the large difference between scales in the x and z directions. In Fig. 4, one can trace three main forms of the beam shape changes: (i) smooth changes of the polarization component amplitudes, which appear to be screwlike variations of the intensity in Figs. 4a and 4c; (ii) beam self-bending (see also Fig. 2); (iii) formation of bright narrow stripes which rise in the beam center and propagate toward the beam rim (the examples of these strips are shown in Fig. 4b by the dotted arrows).

The first type of beam evolution can be explained by coupling between two linearly polarized components of the light wave in the optically active crystal by the photoinduced inhomogeneous linear birefringence. The

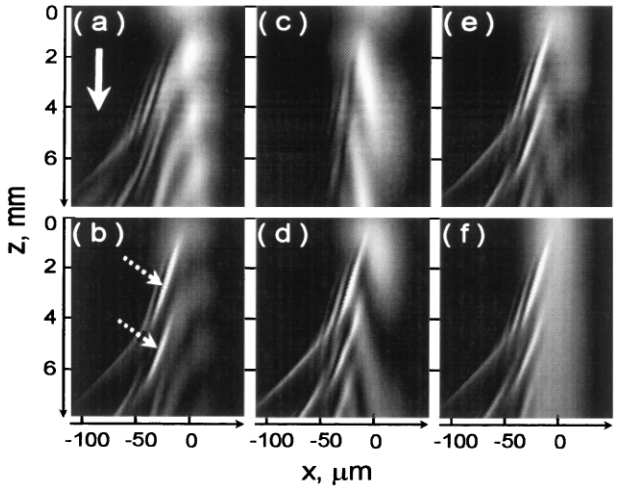

FIG. 4. Numerical simulation of the Gaussian beam propagation in a $Bi_{12}SiO_{20}$ crystal with ac electric field applied along [001] crystalline axes. Panels (a)–(d) show the intensity of two orthogonal polarization components during the positive and negative half-cycle of an ac electric field, $|A_1(x,z)|^2$, $|A_2(x,z)|^2$, $|A_3(x,z)|^2$, and $|A_4(x,z)|^2$, respectively; (e) the intensity of the polarization component orthogonal to the electric field, $|A_2(x,z)^2 + |A_4(x,z)|^2$; (f) the total intensity, $|A_1(x,z)|^2 + |A_2(x,z)|^2 + |A_3(x,z)|^2 + |A_4(x,z)|^2$. The white vertical arrow shows the direction of the light propagation.

spatial period of polarization evolution (polarization beat length) in birefringent optically active crystals is given by $b = \lambda/(\Delta n_l^2 + \Delta n_c^2)$, where Δn_l and Δn_c are the linear and circular birefringence. According to our calculations, during the positive half-cycle of the external field the total electric field has a maximum on the right-hand side of the beam, where the polarization beat length is shorter. The polarization beat length changes in the transverse direction, which produces the screwlike structure shown in Fig. 4. During the negative half-cycle of the external field, the polarization beat length is shorter on the left-hand side of the beam, which leads to another pattern of polarization evolution in the crystal.

When the electric field is along [001] and light propagates along the [110] crystalline axis, the index ellipse has the principal axes in [001] and [1$\bar{1}$0] directions with principal refractive indices $n_1 = n_o$ and $n_2 = n_o - n_o^3 r E(x,z)/2$, respectively. Thus only light polarized orthogonal to the electric field suffers the phase modulation that leads to the separation of the polarization components due to beam self-bending. We have observed this separation experimentally as the beam collapse, when the single beam splits into multiple beams (Fig. 2). To estimate roughly the applied electric field that causes the polarization component separation, we approximate the space charge field in the central part of the beam as $E(x) = \sqrt{2}\,E_0 x/w_0$, where w_0 is the beam-waist dimension. Neglecting the beam deviation inside the crystal, we calculate the electro-optical phase shift for this component as $\phi(x) = \sqrt{2}\,n_o^3 r E_0 L x/\lambda w_0$, that corresponds to the deflection angle $\theta_d \cong n_o^3 r E_0 L/\sqrt{2}\,w_0$. Two polarization components are separated when the deflection angle θ_d exceeds the angular divergence of the Gaussian beam $\theta_G = 2\lambda/\pi w_0$. Comparing θ_d and θ_G, we find that the beam splits into multiple beams when the amplitude of the ac electric field exceeds the value

$$E_C = \frac{2\sqrt{2}\,\lambda}{\pi n_o^3 r L}, \qquad (2)$$

For our BSO sample, Eq. (2) gives $E_C = 1.2$ kV/mm. This value of E_C is almost twice less than we have measured experimentally. The difference is due to optical activity of the crystal that causes the periodic exchange of the light intensity between the polarization components, which reduces the effective length of the crystal. However, the coupling decreases as the electric field increases due to induced linear birefringence. As a result, the deflection angle approaches its estimate by Eq. (2) when the applied field is increased. For the very strong electric fields another factor comes into effect: a considerable increase of the beam transverse dimension due to the spatial separation of the polarization components inside the crystal. This factor leads to a decrease of the electric field gradient; thus it pulls up the beam deflection. The two-fracture dependence of the deflection angle on the applied

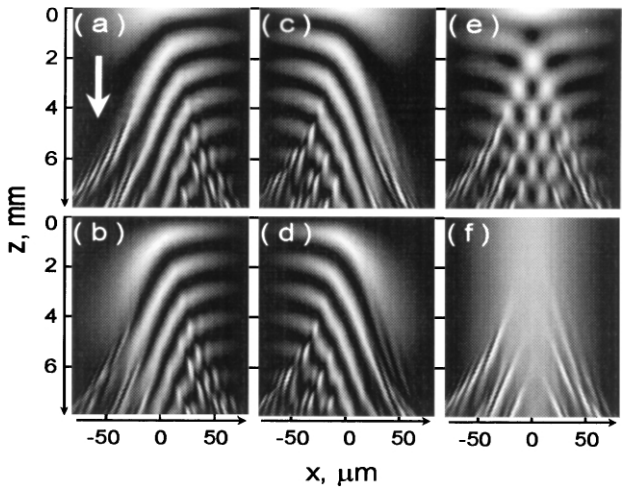

FIG. 5. The same as in Fig. 4, but for an ac electric field applied along a $[1\bar{1}0]$ crystalline axis and for a 100-μm Gaussian beam waist.

electric field (Fig. 2) is the result of the join action of optical activity and the beam dimension changes.

We associate the bright stripes originating near the beam center with a self-channeling of light. These creaselike structures appear in the calculated intensity distributions and have been observed experimentally as well (Fig. 3). Each bright stripe is accompanied by a parallel dark line so the negative gradient of the intensity on both sides from the stripe center causes the positive changes of the refractive index and forms a waveguide. Light is confined within this waveguide if the reflected light interferes constructively with the incident beam. This condition establishes a relation between the strip width, d, and its inclination with respect to the beam propagation direction, $\theta_S = \lambda/2n_o d$. The results of the numerical simulation and experimental data give $\theta_S \approx 0.7°$ and $d \approx 10$ μm when the amplitude of the applied field is 4 kV/mm. The angle θ_S increases with the ac field. We believe that the stripe formation is provoked by the high electric field gradient in a narrow region near the center of the beam. The stripe collapses when it reaches the beam rim. At that point, light from the self-induced waveguide is scattered from the main beam at twice the angle of the stripe inclination (Fig. 4f, bottom left corner). This should be regarded as evidence of light waveguiding in the stripe.

Now we discuss the effect of crystal orientation. Figure 5 shows the results of the numerical simulation of the Gaussian beam propagation in a BSO crystal when the electric field is applied along the $[1\bar{1}0]$ crystalline direction. In this case the angle between the electric field and the principal axes of index ellipse is 45° [17]. The light wave polarized in the direction of the electric field is no longer a normal mode and thus undergoes a strong modulation due to induced linear birefringence. The principal refractive indices are $n_{1,2} = n_o \pm n_o^3 rE(x,z)/2$. In the terms of self-bending this indicates that two waves with orthogonal polarization are deflected by the crystal in opposite directions symmetrically. We have shown by numerical simulation that the weak asymmetry of the light distribution shown in Fig. 5 is due to optical activity.

In conclusion, in this work we have applied BPM to analyze the spatial evolution of the state of polarization of a light beam propagating through a photorefractive crystal, for the first time to our knowledge. We verified the validity of our numerical analysis by a detailed comparison between the numerical and experimental results. We have observed a transverse self-modulation of the beam, the polarization-dependent collapsing of the beam, and the formation of thin inclined self-induced waveguides inside the propagating beam, also for the first time to our knowledge.

We thank R. S. Cudney for stimulating discussions and critical reading of the manuscript. We acknowledge the valuable technical assistance of M. A. García-Zarate. This research was supported by the Consejo Nacional de Ciencia y Tecnología, México, under Projects No. CONACYT/3928P-E and No. 26671-A.

[1] M. Segev, B. Crosignani, A. Yariv, and B. Fischer, Phys. Rev. Lett. **68**, 923 (1992).
[2] H. Meng, H. Salamo, and M. Segev, Opt. Lett. **23**, 897 (1998).
[3] Z. Chen, M. Shih, D. W. Wilson, R. E. Muller, and P. Maker, Opt. Lett. **22**, 1751 (1997).
[4] G. S. García Quirino, M. D. Iturbe Castillo, A. A. Vysloukh, J. J. Sanchez Mondragon, and S. I. Stepanov, Opt. Lett. **22**, 154 (1997).
[5] A. A. Zozulya, M. Saffman, and D. Z. Anderson, Phys. Rev. Lett. **73**, 818 (1994).
[6] G. S. García Quirino, J. J. Sanchez Mondragon, and S. I. Stepanov, Phys. Rev. A **51**, 1571 (1995).
[7] M. Cronin-Golomb, Opt. Lett. **20**, 2075 (1995).
[8] A. V. Khomenko, E. Nippolainen, A. A. Kamshilin, A. Zúñiga Segundo, and T. Jaaskelainen, Opt. Commun. **150**, 175 (1998).
[9] S. I. Stepanov, Rep. Prog. Phys. **57**, 39 (1994).
[10] S. I. Stepanov and M. P. Petrov, Opt. Commun. **53**, 292 (1985).
[11] M. Henry, S. Mallick, D. Rouede, L. E. Celaya, and A. García Weidner, J. Appl. Phys. **59**, 2650 (1986).
[12] A. Brignon and K. H. Wagner, Opt. Commun. **101**, 239 (1993).
[13] Z. Sheng, Y. Cui, N. Cheng, and Y. Wei, J. Opt. Soc. Am. B **13**, 584 (1996).
[14] J. R. Goff, J. Opt. Soc. Am. B **12**, 99 (1995).
[15] D. N. Christodoulides and M. I. Carvalho, Opt. Lett. **19**, 1714 (1994).
[16] See, for example, M. D. Ewbank, R. A. Vazquez, R. R. Neurgaonkar, and J. Feinberg, J. Opt. Soc. Am. B **7**, 2306 (1990).
[17] M. P. Petrov, S. I. Stepanov, and A. V. Khomenko, *Photorefractive Crystals in Coherent Optical Systems* (Springer-Verlag, Berlin, 1991).